Available online at www.sciencedirect.com
ScienceDirect
Carbohydrate Research 342 (2007) 1859–1868
Carbohydrate RESEARCH

Synthesis and conformational analysis of an α-D-mannopyranosyl-(1→2)-α-D-mannopyranosyl-(1→6)-α-D-mannopyranose mimic

Silvia Mari,[a] Inmaculada Sánchez-Medina,[b] Pierangelo Mereghetti,[b] Laura Belvisi,[b] Jesus Jiménez-Barbero[a,*] and Anna Bernardi[b,*]

[a]*Centro de Investigaciones Biológicas, Departamento de Estructura y Functión de Proteínas, CSIC, c/Ramiro de Maeztu 9, 28040 Madrid, Spain*
[b]*Universita' di Milano, Dipartimento di Chimica Organica e Industriale and Centro di Eccellenza CISI, via Venezian 21, 20133 Milano, Italy*

Received 18 January 2007; received in revised form 13 March 2007; accepted 17 March 2007
Available online 24 March 2007

Abstract—A mimic of a (1→2),(1→6)-mannotrioside was synthesized by replacing the central mannose unit with an enantiomerically pure, conformationally stable *trans*-diaxial cyclohexanediol. The three-dimensional structure of the molecule was investigated by NMR spectroscopy supported by molecular modelling and was compared to the known features of the natural mannotrioside.

Keywords: Carbohydrate mimics; Conformational analysis; Glycomimetics; Mannotrioside

1. Introduction

During the past few years, a great deal of research has been concentrated on developing the potential of sugar mimics in different fields of drug discovery.[1–3] Compared to natural carbohydrates, glycomimetics display improved drug-like properties, as they are generally less hydrophilic and less metabolically labile than sugars themselves.

Our approach to the rational design and synthesis of glycomimetics makes use of conformationally stable cyclic diols to replace non-pharmacophoric parts of bioactive oligosaccharides, while preserving the correct orientation of the pharmacophore.[4] This approach has been validated for a 3,4-disubtituted galactose scaffold (a *cis* diol) using as a model system the recognition pair formed by the cholera toxin and ganglioside GM1.[5,6] Supported by adequate experimental work, molecular modelling has also allowed us to make qualitative predictions on the binding mode of new substrates and to design further simplifications of the glycomimetic structure. More recently, we have used the *trans*-diaxial diol **2a** as a mimic of 1,2-substituted α-mannose in the synthesis of a pseudo-mannobioside, which was shown to share the conformational behaviour of its natural counterpart α-Man-(1→2)-α-Man but to be more stable to mannosidase mediated hydrolysis.[7]

We now present our results on the synthesis and conformational analysis of the pseudo-trisaccharide **3**, which was designed as a mimic of the mannotrioside α-Man-(1→2)-α-Man-(1→6)-α-Man- (**1**) by replacing the central mannose moiety with the carbocyclic diol **2**, (1*S*,2*S*,4*S*,5*S*)-4,5-di-methoxycarbonyl-1,2-cyclohexane diol, DCCHD (Fig. 1).[6]

2. Results and discussion

2.1. Synthesis of the mannotrioside mimic 3a

Allyl 2,3,4-tri-*O*-acetyl mannopyranoside **4b** (Scheme 1) was prepared from the known allyl α-D-mannopyranoside[8] in two standard steps. First, selective silylation

* Corresponding authors. Tel.: +39 02 50314092; fax: +39 02 50314072 (A.B.); e-mail addresses: jjbarbero@cib.csic.es; anna.bernardi@unimi.it

0008-6215/$ - see front matter © 2007 Elsevier Ltd. All rights reserved.
doi:10.1016/j.carres.2007.03.019

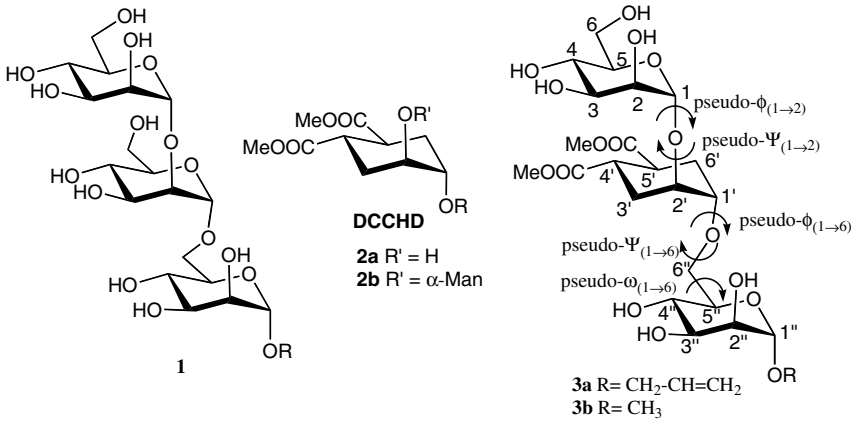

Figure 1. Mannotrioside **1**, DCCHD moiety **2** and mannotrioside mimic **3** structures. Atom numbering and angles definitions are shown for compound **3**; pseudo-$\phi_{(1\rightarrow2)}$: O5–C1–O1–C2′, pseudo-$\Psi_{(1\rightarrow2)}$: C1–O1–C2′–C1′, pseudo-$\phi_{(1\rightarrow6)}$: C6′–C1′–O1′–C6″, pseudo-$\Psi_{(1\rightarrow6)}$: C1′–O1′–C6″–C5″, pseudo-$\omega_{(1\rightarrow6)}$: O1′–C6″–C5″–O5″. The unconventional numbering of the DCCHD moiety in **3** is adopted to facilitate comparison with the natural sugar **1**.

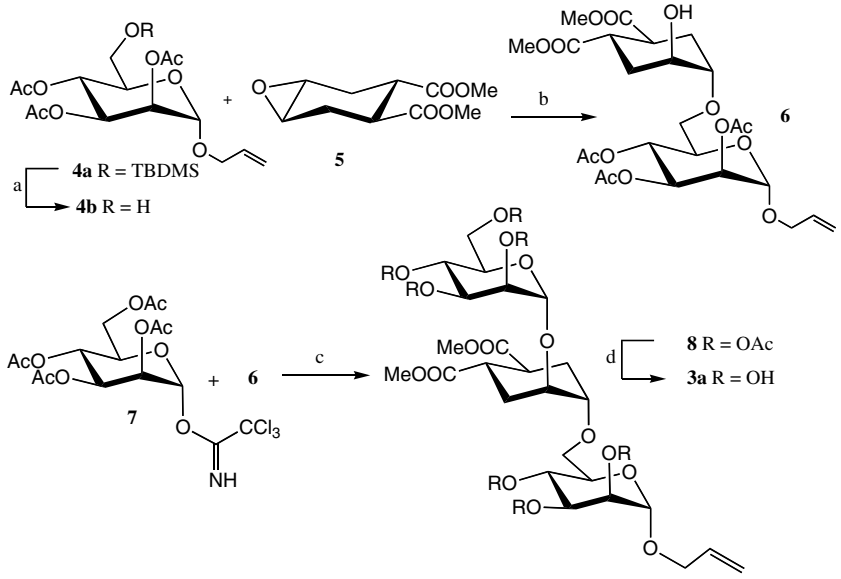

Scheme 1. Synthesis of **3a**. Reagents and conditions: (a) TBAF/AcOH; (b) $Cu(OTf)_2$; (c) TMSOTf; (d) NaOMe, MeOH.

followed by in situ acetylation gave the fully protected **4a**; second, desilylation to give **4b** was performed using a TBAF–AcOH mixture, to avoid the acetyl migration, which took place in the absence of acetic acid. The pseudo α-(1→6)-linked disaccharide **6** was synthesized by Cu-mediated opening of the known epoxide **5**[7] with **4b** (62% yield).

The pseudo-trisaccharide skeleton was then assembled by glycosylation of the acceptor **6** (Scheme 1) with 2,3,4,6-tetra-*O*-acetyl-mannopyranosyl trichloroacetimidate (**7**)[9–11] with TMSOTf (CH_2Cl_2 −20 °C, 20 min, 70%). Deacetylation (NaOMe in MeOH) quantitatively afforded **3a**, whose structure was unequivocally characterized by ^1H and ^{13}C NMR spectroscopy and by mass spectrometry.

2.2. Conformational analysis of the mannotrioside mimic 3

The trisaccharide fragment α-Man-(1→2)-α-Man-(1→6)-α-Man- is one of the terminal arms of the $Man_9GlcNAc_2$ oligosaccharide and copious experimental data on its structure and conformational behaviour are available from X-ray crystallography and NMR spectroscopy.[12,13] Computational studies carried out in our group on the mannotrioside **1** using molecular mechanics and molecular dynamics were found to reproduce the available experimental observations and suggested little correlation between the motion of the (1→2) and (1→6) glycosidic linkages, each tending to behave as they do in the respective (1→2) or (1→6) linked dimannosides.[14]

For the study of the mimic **3b**, the same protocol that proved successful on the natural counterpart was adopted. The analysis began with a stochastic conformational search (Monte Carlo/Energy Minimization, MC/EM), which yielded 195 low-energy conformers within 12 kJ/mol from the global minimum. From these, five separate conformations were extracted that differed for the value of the ω, $\Psi_{(1\rightarrow6)}$ and $\Psi_{(1\rightarrow2)}$ torsion angles and covered the conformational space available to the pseudo-trisaccharide (Fig. 1). These structures were used as the starting point of five separate 5 ns mixed-mode Monte Carlo/Stochastic Dynamics (MC/SD) simulations. The collected output of the dynamic runs (25 ns simulation total, MC/SD set of Table 1) were minimized to obtain the MC/SD/EM set of minima in Table 1. The advantages of such a protocol have been discussed in detail elsewhere.[15]

The results were compared with NMR data obtained by 2D-ROESY spectra acquired at three different mixing time (800, 500 and 200 ms) on a 800 MHz spectrometer.

2.3. The α-Man-(1→2)-DCCHD linkage

The conformation and dynamics of the α-Man-(1→2)-Man linkage have been studied extensively in the oligomannose oligosaccharide $Man_9GlcNAc_2$. Computational[12,14] and experimental[13] results suggest that the linkage exists in two distinct, flexible conformations with similar ϕ value (60°) and different, slowly inter-converting ψ values. The two conformations, which have been termed *S*, for 'stacked', and *E*, for 'extended' (Fig. 2) are both represented in available X-ray structures of mannose oligosaccharides and account for the set of four NOE contacts typically observed across the glycosidic linkage.[13] The H1–H1′ contact (Fig. 2) can arise from conformer *S*, the H5–H1′ and H1–H3′ contacts (Fig. 2) from conformer *E*. The fourth observed NOE contact belongs to the inter-glycosidic H1–H2′ pair, which is at NOE distance in both conformations; the mutually exclusive NOE contacts are marked by blue arrows in Figure 2.

With respect to the pseudo (1→2) linkage, the pseudo-mannotrioside **3** appears to be almost completely represented by extended conformations (pseudo-$\Psi_{(1\rightarrow2)}$ centred at −120°), with a small contribution of the *S* conformation (pseudo-$\Psi_{(1\rightarrow2)}$ centred at −70°) (Figs. 2 and 3b). A continuum motion between the conformers is observed in the dynamic runs (Fig. 3a), but the *S* conformation is still less populated than in the natural sugar. This appears to occur because the *S* conformation of **1** is stabilized by H-bonding interactions involving the two mannose OH6 groups (Fig. 2a), which is lost in the mimic (Fig. 2a′). The same tendency was observed in the conformational behaviour of the pseudo-mannobioside **2b**,[7] but was less pronounced.

As a consequence of the increase in the relative population of the extended conformation *E*, the calculated inter-atomic distances show some differences with those of the natural mannotrioside **1** (Table 1). In particular the H1–H1′ distance becomes longer ($\geqslant$3.9 Å), reaching the NOE limit (see Table 1). The predominance of the extended conformation *E* is confirmed by 2D ROESY experiments where the intensities of the *S* conformer-exclusive NOE contact H1–H1′ and of the *E* conformer-exclusive NOE contact H1–H3′eq were found

Table 1. Calculated and experimental inter-proton distances (Å) for pseudo-mannotrioside **3**, in comparison with those of the natural mannotrioside **1** and with the NOE contacts observed for **2b**

Linkage	Proton pair	**3** MC/SD[a] MC/SD/EM[b] Distance (Å)	3 Exp. distances (ISPA Model, Å)[c]	**2b** NOE intensity from NOESY spectrum[d]	**1** Exp. distance range[e]
α (1→2)	H_1–H'_1	4.0 4.0	3.2	Weak NOE	2.8–3.2
	H_1–H'_2	2.4 2.3	2.3	Strong NOE	2.0–2.4
	H_1–H'_{3eq}	2.9 2.8	2.7	Strong NOE	—
	H_1–H'_{3ax}	4.0 4.1	$\geqslant$4	Not detectable	3.1–3.8
	H_5–H'_1	2.7 2.3	—[f]	Strong NOE	2.3–2.9
	H'_{1-4}	4.0 4.1	3.6	Weak NOE	>3.5

[a] Distances calculated from $<r^{-6}>$ monitored during the simulation.
[b] Multi-conformer minimization of the dynamic snapshots.
[c] Distances for compound **3** derived using the isolated spin-pair approximation (ISPA) by comparing relative NOE intensities. Error estimation in the measurement is ±0.2 Å.
[d] From Ref. 7.
[e] Distance range for compound **1** from experimental data.[12]
[f] Distances not measurable due to signal overlap.

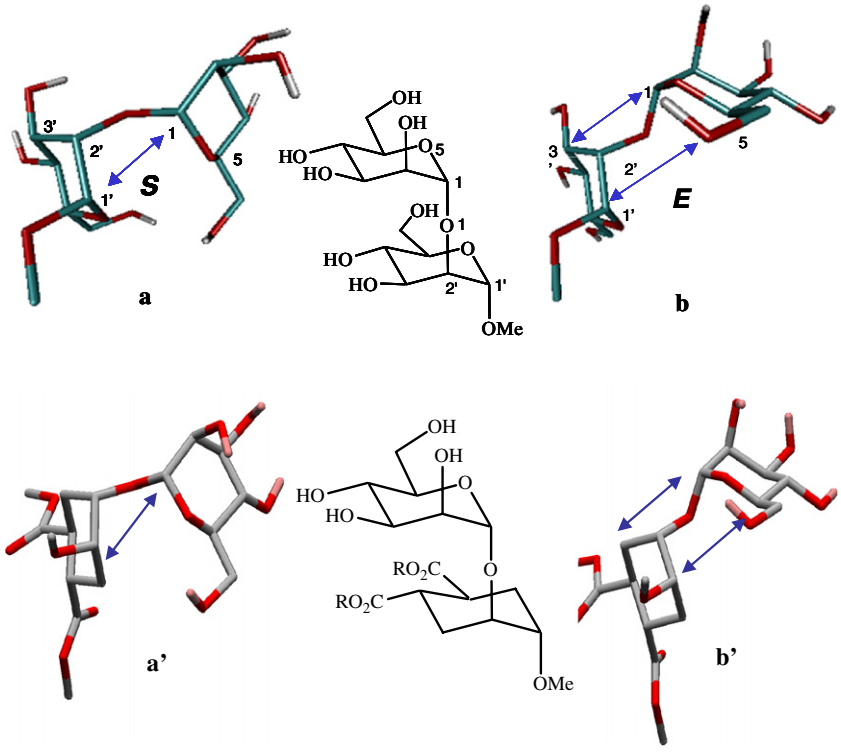

Figure 2. Low-energy conformations of the (1→2)-mannobioside (a, b) and of the pseudo-mannobioside fragment of **3** (a′,b′). **a**, **a**′, The stacked conformation *S* (Φ, Ψ 88°, −58°); **b**, **b**′. The extended conformation *E* (Φ, Ψ 72°, −138°). Characteristic NOE contacts are indicated by the blue arrows.

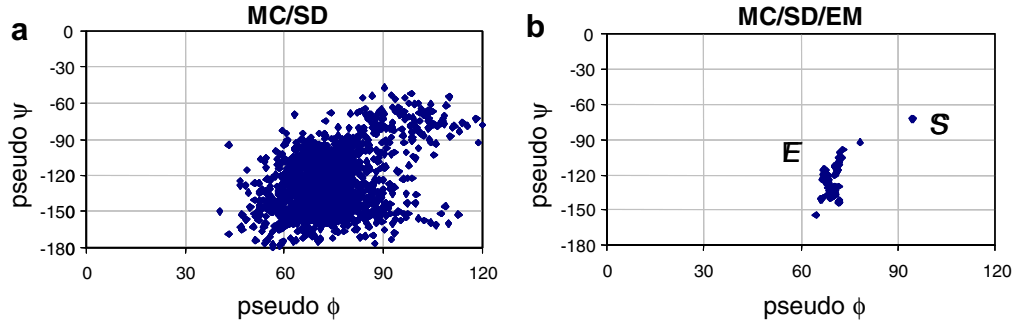

Figure 3. Conformational studies on the pseudo (1→2) linkage in the pseudo-mannotrioside **3**. Pseudo-$\phi_{(1\rightarrow2)}$: O5–C1–O1–C2′; pseudo-$\Psi_{(1\rightarrow2)}$: C1–O1–C2′–C1′ (numbering of the DCCHD moiety is shown in Fig. 1). Calculations were run with MMOD 7.0, using AMBER* and the Generalized Born/Surface Area (GB/SA) water solvation model. (a). 5 ns of MC/SD dynamics simulation; (b). Minimization of the structures saved during the dynamics runs (MC/SD/EM calculations).

to be 0.46% and 1.97%, respectively (see Supplementary data, Table S-2 for details). Furthermore, a medium intensity NOE contact between H2′ and H5 (corresponding isolated spin-pair approximation (ISPA) distance of 2.9 Å ± 0.2) is in accordance with a pseudo-$\Psi_{(1\rightarrow2)}$ torsion angle centred at −130° as expected for the *E* cluster (see Fig. 2 and Table 3).

2.4. The DCCHD-(1→6)-α-Man linkage

The (1→6) linkage of natural mannotrioside **1** was found to populate a single conformation of the exo-anomeric torsion angle ϕ, with a ϕ value centred around 60°; two states were found for Ψ (180° and 90°) and ω (gt, $\omega = 60°$ and gg, $\omega = -60°$).[14] Experimentally, the linkage is described as flexible, with a 3–4:1 mixture of gg and gt conformers around ω and two values accessible for Ψ.[12,16]

The conformational maps obtained from dynamic simulations of mimic **3** are somewhat more complex, and yield the picture of a rather flexible fragment (the details have been collected in the Supplementary data). The main difference between **3** and its natural counterpart **1** arises from the loss of the exo-anomeric effect in the mimic. The conformational distribution of the pseudo-

exo-anomeric torsion in **3**, pseudo-ϕ, which in the natural mannotrioside is fixed around 60°, is calculated to vary almost continuously in the range 80–160°. Furthermore, in **3**, the gt conformation of the pseudo-ω torsion angle is calculated to be largely prevailing with only some contribution from the gg and tg conformers (the pseudo-ω angle: O1′–C6″–C5″O5″ is defined in Fig. 1). Destabilization of the gg cluster relative to the natural sugar may be correlated to the destabilization of the stacked conformation *S* of the (1→2) linkage, because in the natural trisaccharide the gg cluster was formed mainly by stacked (1→2) conformers. The pseudo-Ψ torsion angle of **3** (pseudo-$\Psi_{(1\rightarrow6)}$: C1′–O1′–C6″–C5″, see Fig. 1) is represented by three states (−90°, 180°, +90°), rather than two (180° and 90°).

The inter-atomic distances for the critical proton pairs, $H'_1 - H''_{6a}$, $H'_1 - H''_{6b}$, $H'_1 - H''_5$, $H'_2 - H''_{6a}$ and $H'_2 - H''_{6b}$, that are obtained from the dynamics are reported in Table 2. Quantitative experimental data could not be obtained directly from **3**, because the signals of the relevant protons severely overlap, even at 800 MHz. However, it clearly appears from the reported intensities of the NOE cross-peaks that the simulation of the (1→6) linkage dynamics does not correspond to the experimental observations (Table 2). In particular, no cross-peaks could be observed in the NMR spectra for the $H'_1 - H''_{6b}$ and $H'_2 - H''_{6b}$ proton pairs, whereas a significant NOE signal would be expected based on the calculated distances of 2.4 Å. It is worth noting that a short $H'_1 - H''_{6b}$ distance (2.0–2.3 Å) is reported for the natural trimannoside **1**.

To achieve a qualitative picture from the available NMR data, we attempted to define geometrical restrictions and compare them with the characteristics of the conformational clusters obtained from minimization of the dynamic simulations snapshots. Minimization of the structures saved during the MC/SD dynamics runs yielded 81 structures within 12 kJ/mol (MC/SD/EM set), which could be classified as a combination of the eight different conformations shown in Figure 4. All the low-energy conformers belong to the extended family of the (1→2) linkage, and the first stacked conformation is found just above 10 kJ/mol. The gg population is also low, most gg conformers are (1→2) stacked (*S*) and higher in energy. Conformations within the first 10 kJ/mol (no (1→2) stacked conformations included) have been reported in the three-dimensional plot of Figure 5 (pseudo-$\phi_{(1\rightarrow6)}$, pseudo-$\Psi_{(1\rightarrow6)}$, pseudo-$\omega_{(1\rightarrow6)}$). They give rise to six clusters with two states for ω (gt and gg), three for ϕ (150°, 120°, 90°), five for Ψ (−90°, −140°, 120°, 180°, 90°).

The conformational features and the associated values for critical inter-proton distances of the eight cluster leaders are collected in Table 3. The geometrical restrictions that could be deduced from the NMR data were compared to these values to identify the conformation(s) most represented in solution.

The preferred conformation of the pseudo-$\omega_{(1\rightarrow6)}$ angle could be established based on coupling constant analysis. Protons $H6''_a$ (at 3.87 ppm) and $H6''_b$ (at 3.74 ppm) appear respectively as a doublet ($J_{6''a,6''b} =$ 12 Hz, $J_{6''a,5''} \leqslant 2$ Hz) and a triplet ($J_{6''a,6''b} = J_{6''a,5''} =$ 12 Hz), which implies an exclusive anti orientation for $H6''_b$ relative to H5″, and a syn orientation for $H6''_a$. This is in agreement with the gt conformation expected based on the modelling prediction (see Table 3), and departs from the gg:gt mixture observed for the natural disaccharide.

Table 2. Observed NOE contacts and calculated inter-proton distances (Å) for pseudo-mannotrioside **3**, in comparison with those of the natural mannotrioside **1**

Linkage	Proton pair	**3** MC/SD[a] (MC/SD/EM)[b] Distance (Å)	**3** NOE intensity	**1** MC/SD[a] (MC/SD/EM)[b] Distance (Å)	**1** Exp. distances range[c]
α (1→6)	H'_1–H''_{6a}	2.7 (3.0)	Strong NOE[d]	3.0 (2.9)	2.2–2.7
	H'_1–H''_{6b}	2.5 (2.4)	No NOE	2.5 (2.5)	2.0–2.3
	H'_1–H''_5	4.1 (3.3)	—[d]	3.9 (2.6)	[e]
	H'_2–H''_{6a}	—[f] (3.1)	Strong (2.81 Å)[g]		[e]
	H'_2–H''_{6b}	—[f] (2.4)	No NOE		[e]

[a] Calculated from $\langle r^{-6} \rangle$ monitored during the simulation.
[b] Multi-conformer minimization of the dynamic snapshots.
[c] Distance range for compound **1** from experimental data.[12]
[d] Distances not measurable due to signal overlap.
[e] Not reported.
[f] Not monitored.
[g] Distance evaluated from the isolated spin-pair approximation (ISPA).

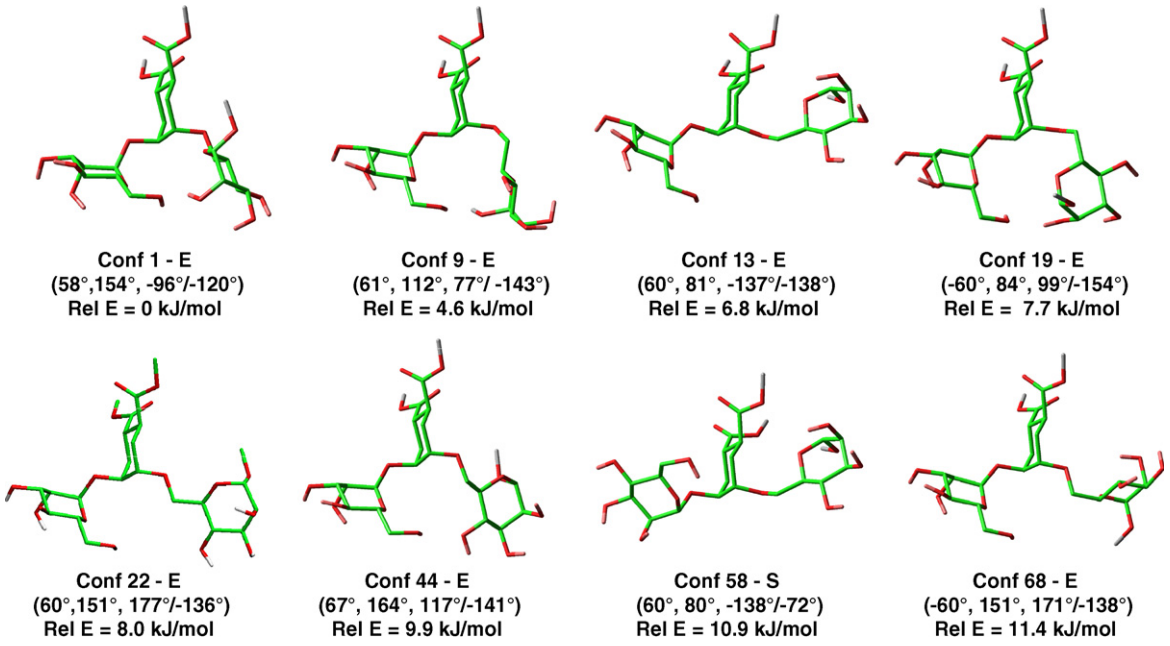

Figure 4. Conformational studies on pseudo-mannotrioside **3b**. Low-energy conformations (12 kJ/mol from the global minimum) from the MC/SD/EM calculations. (Numbering of the DCCHD moiety as in Fig. 1.) The lowest energy member of each cluster is shown. The data in parentheses are the values of the pseudo-ω, $\phi_{(1\rightarrow6)}$, $\Psi_{(1\rightarrow6)}/\Psi_{(1\rightarrow2)}$ torsion angles (ω: O1′–C6″–C5″–O5″; $\phi_{(1\rightarrow6)}$: C6′–C1′–O1′–C6″; $\Psi_{(1\rightarrow6)}$: C1′–O1′–C6″–C5″; $\Psi_{(1\rightarrow2)}$: C1–O1–C2′–C1′).

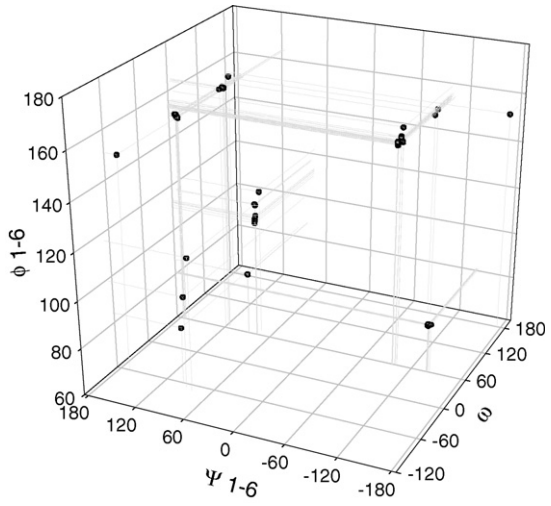

Figure 5. MC/SD/EM set of conformers for **3b**: ω, $\Psi_{(1\rightarrow6)}/\phi_{(1\rightarrow6)}$ torsion angles plots (pseudo-$\phi_{(1\rightarrow6)}$: C6′–C1′–O1′–C6″, pseudo-$\Psi_{(1\rightarrow6)}$: C1′-O1′-C6″-C5″, pseudo-$\omega_{(1\rightarrow6)}$: O1′–C6″–C5″–O5″). The points represent the conformers located within the first 10 kJ/mol.

Analysis of the pseudo-inter-glycosidic distances is based on three sets of NOE contacts between the H6″ protons and protons 2′, 1′ and 6′ of the DCCHD ring. The H6′eq proton (Fig. 6) does not show NOE contacts with either $H6''_a$ or $H6''_b$, which suggests proton distances $\geqslant$4 Å. As listed in Table 3, this condition is satisfied by conformers 1, 22, 44 and 68, and can be translated into a pseudo-$\phi_{(1\rightarrow6)}$ value centred around 150°. Conformer 68, however, does not belong to the gt family of pseudo-$\omega_{(1\rightarrow6)}$ conformers and cannot account for the coupling constant analysis discussed above. The remaining three conformations, 1, 22 and 44 can be discriminated by looking at the experimentally observed NOE contacts between the remaining sets of protons. Both H1′ and H2′ show a strong NOE contact with $H6''_a$, and a very weak NOE contact with $H6''_b$ (Fig. 6). This behaviour is fully represented only by conformer 44. So, the available NMR results could be interpreted based on a major conformation of the (1→6) linkage corresponding to conformer 44 of Table 3, which features the following values for the inter-glycosidic torsion angles: pseudo-$\omega_{(1\rightarrow6)} = 60°$ (gt family), pseudo-$\phi_{(1\rightarrow6)} = 164°$, pseudo-$\Psi_{(1\rightarrow6)} = 117°$. At this qualitative level, it cannot be discounted that an appropriate combination of all, or some of the pseudo-$\omega_{(1\rightarrow6)}$ gt conformers could be generating the experimental values of the observables. To explore this possibility, the conformer population was estimated by fitting to the NOE intensity values using a procedure already reported[17] and described in detail in the Supplementary data. In the present case, the estimate is rather approximate because the spectral overlap makes the intensity of the NOE cross-peaks hard to evaluate quantitatively. However, the results show that the experimental data can be also fitted if conformer 44 coexists in dynamic equilibrium with approximately 10% of conformer 22, which features the following values for the inter-glycosidic torsion angles: pseudo-$\omega_{(1\rightarrow6)} = 60°$ (gt family), pseudo-$\phi_{(1\rightarrow6)} = 151°$,

Table 3. Geometrical parameters for the eight leading conformers of **3** represented in Figure 4

	Conf. 1	Conf. 9	Conf. 13	Conf. 19	Conf. 22	Conf. 44	Conf. 58	Conf. 68
E_{rel} (kJ/mol)	0.0	4.6	6.8	7.7	8.0	9.9	10.9	11.4
pseudo-$\Psi_{(1\rightarrow2)}$	−120°	−140°	−130°	−154°	−136°	−141°	−72°	−138°
$d_{H2'-H5}$ (Å)	3.54	3.26	3.30	2.86	3.29	3.13	4.43	3.26
pseudo-$\omega_{(1\rightarrow6)}$	58° (**gt**)	61° (**gt**)	60° (**gt**)	−60° (gg)	60° (**gt**)	67° (**gt**)	60° (**gt**)	−60° (gg)
pseudo-$\phi_{(1\rightarrow6)}$	154°	112°	81°	84°	151°	164°	80°	151°
pseudo-$\Psi_{(1\rightarrow6)}$	−96°	77°	−137°	99°	175°	117°	−138°	171°
$d_{H6'eq-H6''a}$ (Å)	**4.59**	2.86	3.81	2.32	**4.40**	**4.18**	3.79	**4.40**
$d_{H6'eq-H6''b}$ (Å)	**4.26**	3.84	2.29	3.29	**3.70**	**4.15**	2.28	**3.70**
$d_{H2'-H6''a}$ (Å)	3.29	4.27	4.24	4.24	**2.29**	**2.34**	3.94	**2.28**
$d_{H2'-H6''b}$ (Å)	2.28	4.03	3.92	4.60	**3.50**	**3.76**	4.28	**3.59**
$d_{H1'-H6''a}$ (Å)	3.54	**2.29**	2.86	**2.33**	2.67	**2.23**	2.83	2.59
$d_{H1'-H6''b}$ (Å)	2.35	**3.49**	2.31	**3.54**	2.34	**3.12**	2.31	2.40

Values of pseudo-$\omega_{1\rightarrow6}$ and interproton distances that qualitatively agree with the experimental observations are highlighted in bold (ω: O1′–C6″–C5″–O5″; $\phi_{(1\rightarrow6)}$: C6′–C1′–O1′–C6″; $\Psi_{(1\rightarrow6)}$: C1′–O1′–C6″–C5″; $\Psi_{(1\rightarrow2)}$: C1–O1–C2′–C1′).

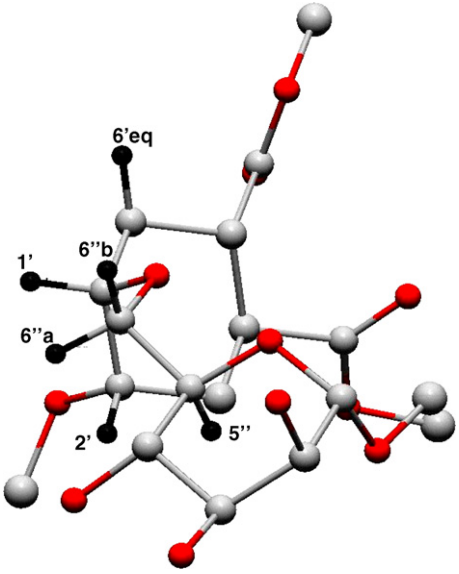

Figure 6. Close-up view of the (1→6) glycosidic linkage in a conformation that satisfies all NMR restraints.

pseudo-$\Psi_{(1\rightarrow6)} = 175°$. Inclusion of all other conformations located by the conformational search produce larger deviation from the experimental data. Based on this analysis, therefore, the only flexibility of the pseudo-(1→6) linkage is limited to the pseudo-$\Psi_{(1\rightarrow6)}$ torsion.

2.5. Conclusions

The α-Man-(1→2)-α-Man-(1→6)-α-Man-trisaccharide **1** is one of the arms of the $Man_9GlcNAc_2$ oligosaccharide. Experimental data from X-ray and NMR spectroscopy[13] have allowed its description as a rather flexible element, which can sample multiple conformations, of both the (1→2) and the (1→6) fragments. The pseudo-trisaccharide **3** was devised as a structural mimic of **1**, and the work described here has allowed us to experimentally evaluate the conformational behaviour of **3** and its similarity to the natural template. The collection and analysis of the NMR data was complicated by the severe spectral overlap, but ROESY spectra obtained at 800 MHz and interpreted on the basis of structural models derived from molecular dynamics simulations allowed us to obtain a qualitative identification of the most relevant conformational features of the mimic. The picture of **3** emerging from this study is of a molecule in some sense more rigid than the natural trisaccharide. The (1→2)-linked fragment, which in **1** can be either in the stacked (*S*) or in the extended (*E*) conformation is represented in **3** mostly by *E* conformers. This feature is captured well by the molecular mechanics and dynamics calculations. The experimental data also clearly indicate a strong restriction of the (1→6)-linkage that was not expected based on the computational predictions. In particular, the coupling constants analysis of the H5–H6 proton couplings is only compatible with a gt conformation for the pseudo-ω dihedral angle. Concerning the remaining degrees of freedom pseudo-$\phi_{(1\rightarrow6)}$ and pseudo-$\psi_{(1\rightarrow6)}$, the observed inter-glycosidic NOE contacts could be interpreted as arising either from one single conformation (number 44 of Fig. 4) showing no violations of the NOE constraints or, more likely, from a 90:10 mixture of conformers 44 and 22 (Fig. 4) in rapid equilibrium. In any case, this corresponds to a preferred conformation for the pseudo-$\phi_{(1\rightarrow6)}$ dihedral angle at ca $155 \pm 5°$, whereas some residual flexibility is observed for pseudo-$\psi_{(1\rightarrow6)}$ (117° in 44 and 175° in 22). Compared to the natural trisaccharide **1**, therefore, the pseudo-(1→6) linkage of **3** appears to be less flexible and locked in the unnatural pseudo-$\phi_{(1\rightarrow6)}$ 155° conformation.

3. Experimental

3.1. Synthesis

NMR spectra were recorded at 25 and 30 °C on Bruker spectrometers. The cyclohexanediol moiety is numbered as in Figure 1. Chemical shifts ^{1}H and ^{13}C NMR spectra are expressed in ppm relative to TMS or to DSS for spectra recorded in D_2O. Numbering of the spectra as shown in Figure 1. Mass spectrometry was performed with a VG 7070 EQ-HF apparatus (FAB ionization), or an Omniflex apparatus (MALDI ionization). Optical rotations $[\alpha]_D$ were measured in a 1-dm path-length cell with 1 mL capacity on a Perkin–Elmer 241 polarimeter. Thin layer chromatography (TLC) was carried out with precoated Merck F254 silica gel plates. Flash chromatography (FC) was carried out with Macherey-Nagel silica gel 60 (230–400 mesh). Solvents were dried by standard procedures and reactions requiring anhydrous conditions were run under nitrogen. The epoxide **5**[7] and the trichloroacetimmidate **7**[9–11] were prepared by published procedures. Allyl α-D-mannopyranoside is a known compound.[8]

3.1.1. Allyl 2,3,4-tri-*O*-acetyl-6-*O*-*t*-butyldimethylsilyl-α-D-mannopyranoside (4a). To a solution of allyl α-D-mannopyranoside[8] (1.08 g, 4.9 mmol) in dry pyridine (15 mL) TBDMSCl (818 mg, 5.43 mmol) was added, at 0 °C. The mixture was stirred at rt for 72 h and the reaction monitored by TLC ($CHCl_3$–MeOH, 8:2). When the starting material had disappeared, Ac_2O (2.2 mL) was added and stirring was continued overnight. After 17 h the mixture was concentrated, the residue dissolved in EtOAc and washed with 3 N HCl, saturated $NaHCO_3$ and water. The organic phase was dried over Na_2SO_4 and evaporated. The crude was purified by flash chromatography (hexane–EtOAc 8:2) to give **4a** (1.5 g, 65%) as a colourless oil. $[\alpha]_D^{20}$ +43.4 (*c* 1.5, $CHCl_3$); ^{1}H NMR (400 MHz, C_6D_6): δ 0.16 (s, 6H, $Si(CH_3)_2$), 1.09 (s, 9H, $C(CH_3)_3$), 1.78 (s, 3H, $OCOCH_3$), 1.82 (s, 3H, $OCOCH_3$), 1.84 (s, 3H, $OCOCH_3$), 3.82 (m, 2H, H_6), 3.85–3.89 (m, 1H, CH_2–CH=CH_2), 4.05 (m, 1H, H_5), 4.11 (dd, 1H, CH_2–CH=CH_2, $J_{gem} = 13$ Hz, $J_{vic} = 5$ Hz), 4.89 (d, 1H, H_1, $J_{1,2} = 1.8$ Hz), 5.10 (app d, 1H, CH_2–CH=CH_2, $J_{vic} = 10.4$ Hz), 5.27 (app d, 1H, CH_2–CH=CH_2, $J_{vic} = 17$ Hz), 5.63 (m, 1H, H_2), 5.73–5.85 (m, 1H, CH_2–CH=CH_2), 5.78 (m, 1H, H_3), 5.81 (m, 1H, H_4); ^{13}C NMR (50.3 MHz, C_6D_6): δ −4.59 (2 × CH_3), 19.1 (CMe_3), 21 (3 × CH_3), 26.7 (3 × $COCH_3$), 63.2 (C6), 67.3 (C3), 68.8 (CH_2–CH=CH_2), 70.7 (C4), 70.9 (C2), 72 (C5), 97.5 (C1), 118.2 (CH_2–CH=CH_2), 134.3 (CH_2–CH=CH_2), 169.8 (MeCO), 170.3 (2 × MeCO); MS (FAB^+) $[M-OCH_2-CH=CH_2]^+$: 403.

3.1.2. Allyl 2,3,4-tri-*O*-acetyl-α-D-mannopyranoside (4b). At 0 °C, under N_2, HOAc (567 μL, 9.9 mmol) was added dropwise to a solution of **4a** (912 mg, 1.98 mmol) in dry THF (20 mL), the solution was warmed to rt and a solution of TBAF (1 M in THF, 2.37 mL, 2.37 mmol) was added. The mixture was stirred overnight under N_2 at rt (TLC hexane–EtOAc, 1:1). Brine was added and the solution was extracted several times with EtOAc. The combined organic phases were dried over Na_2SO_4, and the solvent was removed. The product was purified by flash chromatography (hexane–EtOAc, 4:6) to give **4b** (588 mg, 86%) as yellow oil. $[\alpha]_D^{20}$ +53.7 (*c* 1.0, $CHCl_3$); ^{1}H NMR (400 MHz, $CDCl_3$): δ 1.97 (s, 3H, $OCOCH_3$), 2.04 (s, 3H, $OCOCH_3$), 2.11 (s, 3H, $OCOCH_3$), 3.58 (dd, 1H, H_{6a}, $J_{gem} = 13$ Hz, $J_{5,6a} = 4$ Hz), 3.68 (dd, 1H, H_{6b}, $J_{gem} = 13$ Hz, $J_{5,6b} = 2$ Hz), 3.77 (m, 1H, H_5), 4.00 (dd, 1H, CH_2–CH=CH_2, $J_{gem} = 13$ Hz, $J_{vic} = 4$ Hz), 4.18 (dd, 1H, CH_2–CH=CH_2, $J_{gem} = 13$ Hz, $J_{vic} = 6$ Hz), 4.85 (d, 1H, H_1, $J_{1,2} = 2$ Hz), 5.21 (t, 1H, H_4, $J = 10$ Hz), 5.25 (m, 1H, H_2), 5.26–5.31 (m, 2H, CH_2–CH=CH_2), 5.38 (dd, 1H, H_3, $J_{2,3} = 3$ Hz, $J = 10$ Hz), 5.81–5.92 (m, 1H, CH_2–CH=CH_2); ^{13}C NMR (50.3 MHz, HETCOR, $CDCl_3$): δ 21 (3 × $COCH_3$), 62 (C6), 67 (C4), 68 (CH_2–CH=CH_2), 69.5 (C3), 70.5 (C2), 97.5 (C1), 119.5 (CH_2–CH=CH_2), 134 (CH_2–CH=CH_2); MS (FAB^+) $[M-OCH_2-CH=CH_2]^+$: 289.

3.1.3. Dimethyl (1*S*,2*S*,4*S*,5*S*)-4-hydroxy-5-[6-(1-allyl-2,3,4-tri-*O*-acetyl-α-D-mannopyranosyl)]-cyclohexane-1,2-dicarboxylate (6). A solution of **4b** (1.45 g, 4.20 mmol) in CH_2Cl_2 (3 mL) was added to **5**[7] (300 mg, 1.40 mmol). Then $Cu(OTf)_2$ (50.6 mg, 0.14 mmol) was added. The reaction was stirred overnight under N_2 at rt (TLC $CHCl_3$–acetone, 92:8) before adding a pH 9 NH_4Cl/NH_4OH solution. The phases were separated. The organic phase was washed several times with saturated NH_4Cl and the combined aqueous phases were extracted with AcOEt. The combined organic phases were dried and concentrated. The crude was purified by flash chromatography ($CHCl_3$–acetone, 95:5) to give **6** (488 mg, 62%) as pale yellow oil. $[\alpha]_D^{20}$ +55.42 (*c* 1.3, $CHCl_3$); ^{1}H NMR (400 MHz, C_6D_6): δ 1.74–1.87 (s, 12H, 4 × $OCOCH_3$), 1.95–2.05 (m, 1H, $H_{3'ax}$), 2.11–2.19 (m,2H, $H_{6'eq}$, $H_{6'ax}$), 2.25–2.35 (m, 1H, $H_{3'eq}$), 3.35–3.41 (m, 2H, $H_{4'}$, $H_{5'}$), 3.40 (s, 6H, 2 × OCH_3), 3.50 (m, 1H, $H_{1'}$), 3.60 (dd, 1H, $H_{6''a}$, $J_{gem} = 11$ Hz, $J_{vic} = 2.5$ Hz), 3.73 (dd, 1H, $H_{6''b}$, $J_{gem} = 11$ Hz, $J_{vic} = 5$ Hz), 3.85–3.91 (m, 2H, $H_{2'}$, CH_2–CH=CH_2), 4.05–4.15 (m, 2H, $H_{5''}$, CH_2–CH=CH_2), 4.91 (d, 1H, $J_{1,2} = 1.6$ Hz, $H_{1''}$), 5.18 (app d, 1H, $J = 10.4$ Hz, CH_2–CH=CH_2), 5.35 (app d, 1H, $J = 17$ Hz, CH_2–CH=CH_2), 5.72 (m, 1H, $H_{2''}$), 5.73–5.90 (m, 3H, CH_2–CH=CH_2, $H_{3''}$, $H_{4''}$); ^{13}C NMR (37.7 MHz, $CDCl_3$): δ 20.8 (3 × $COCH_3$), 27.1 (C6′), 30.4 (C6″), 39.1 (C4′), 39.4 (C5′), 51.9 (2 × OMe), 66.6 (C2′), 67.7

(C6″), 68.5 (CH_2–CH=CH_2), 69.2, 69.6, 69.9, 78.2 (C1′), 96.4 (C1″), 118.1 (CH_2–CH=CH_2), 133.1 (CH_2–CH=CH_2), 169.8, 174.6; MALDI-TOF $[M+Na]^+$: 583.65.

3.1.4. Dimethyl (1*S*,2*S*,4*S*,5*S*)-4-[1-α-(2,3,4,6-tetra-*O*-acetyl-D-mannopyranosyl)]-5-[6-(1-allyl-2,3,4-tri-*O*-acetyl-α-D-mannopyranosyl)]-cyclohexane-1,2-dicarboxylate (8). The alcohol **6** (88.3 mg, 0.157 mmol) was mixed with 4 Å molecular sieves and dried in vacuo overnight, then the trichloroacetimidate **7**[9–11] (131.5 mg, 0.267 mmol) in CH_2Cl_2 (4 mL) and was added under N_2. The mixture was cooled at −20 °C, stirred for approximately 15 min and TMSOTf (11.4 μL) was added. The stirring was continued at −20 °C for 50 min (TLC $CHCl_3$–acetone, 92:8). The reaction was neutralized by adding triethylamine and concentrated. The product was isolated by flash chromatography ($CHCl_3$–acetone, 95:5) to give **8** (98.9 mg, 71%) as a colourless oil. $[\alpha]_D^{20}$ +24.9 (*c* 1.2, $CHCl_3$); ^{1}H NMR (400 MHz, C_6D_6): δ 1.71 (s, 3H, $OCOCH_3$), 1.77 (s, 6H, 2 × $OCOCH_3$), 1.79 (s, 3H, $OCOCH_3$), 1.81 (s, 3H, $OCOCH_3$), 1.88 (s, 3H, $OCOCH_3$), 1.90 (s, 3H, $OCOCH_3$), 1.95–2.25 (m, 4H, $H_{3'}$, $H_{6'}$), 3.21–3.32 (m, 2H, $H_{4'}$, $H_{5'}$), 3.39 (s, 3H, OCH_3), 3.40 (s, 3H, OCH_3), 3.55–3.65 (m, 2H, $H_{6a''}$, $H_{1'}$), 3.72 (dd, 1H, $H_{6b''}$, $J_{gem} = 13$ Hz, $J_{vic} = 6$ Hz), 3.93 (dd, 1H, $J_{gem} = 13$ Hz, $J_{vic} = 6$ Hz, CH_2–CH=CH_2), 4.0–4.05 (m, 1H, $H_{2'}$), 4.09–4.19 (m, 2H, $H_{5''}$, CH_2-CH=CH_2), 4.23–4.31 (m, 1H, H_5), 4.35 (app d, 1H, $J = 10$ Hz, H_{6a}), 4.45 (dd, 1H, $J = 10$ Hz, $J_{vic} = 5.5$ Hz, H_{6b}), 4.90 (br s, 1H, $H_{1''}$), 5.09 (br s, 1H, H_1), 5.11–5.21 (m, 1H, CH_2–CH=CH_2), 5.36 (app d, 1H, $J = 10$ Hz, CH_2–CH=CH_2), 5.59 (m, 1H, H_2), 5.71 (m, 1H, $H_{2''}$), 5.70–5.90 (m, 5H, H_4, H_3, $H_{3''}$, $H_{4''}$, CH_2–CH=CH_2); ^{13}C NMR (50.3 MHz, C_6D_6): δ 20.3 (7 × $CO\mathit{C}H_3$), 27, 28, 39.5 (C4′, C5′), 51.6 (2 × OMe), 62.9 (C6″), 66.9, 67.1, 68.7, 68.9, 69.6, 70.1, 70.4, 70.6, 70.8, 72.9 (C2′), 75.7 (C1′), 96.2 (C1″), 97.2 (C1), 117.8 (CH_2–CH=CH_2), 133.8 (CH_2–CH=CH_2), 169.7, 175; MALDI-TOF $[M+Na]^+$: 914.61.

3.1.5. Dimethyl (1*S*,2*S*,4*S*,5*S*)-4-(1-α-D-mannopyranosyl)-5-[6-(1-allyl-α-D-mannopyranosyl)]-cyclohexane-1,2-dicarboxylate (3a). Under N_2, a 1 M MeOH solution of NaOMe (25 μL) was added to a solution of **8** (18.1 mg, 0.02 mmol) in dry MeOH (1 mL). The mixture was stirred at rt for 15 min, while monitoring the reaction by TLC ($CHCl_3$–MeOH, 9:1). The mixture was neutralized with Amberlite IR 120 H^+ and the resin was removed by filtration. After washing the resin with MeOH, the combined filtrate was concentrated under vacuum to give pure **3a** (12.4 mg, quantitative) as colourless oil. $[\alpha]_D^{20}$ +75.61 (*c* 0.9, CH_3OH); ^{1}H NMR (500 MHz, D_2O): δ 1.70–1.82 (m, 2H, $H_{3'ax}$, $H_{6'ax}$), 2.08–2.18 (m, 2H, $H_{3'eq}$, $H_{6'eq}$), 2.91 (m, 2H, $H_{4'}$, $H_{5'}$), 3.52–3.60 (m, 3H, H_4, $H_{5''}$, H_5), 3.65 (s, 3H, OCH_3), 3.66 (s, 3H, OCH_3), 3.65–3.72 (m, 5H, $H_{4''}$, H_{6b}, $H_{3''}$, $H_{1'}$, $H_{6b''}$), 3.77 (m, 1H, H_3), 3.81 (app d, 2H, $J = 11$ Hz, $H_{6a''}$, H_{6a}), 3.89 (dd, 1H, $J_{2'',3''} = 3.4$ Hz, $J_{2'',1''} = 1.7$ Hz, $H_{2''}$), 3.93 (dd, 1H, $J_{2,3} = 3.3$ Hz, $J_{2,1} = 1.7$ Hz, H_2), 3.97 (app q, 1H, $J = 3$ Hz, $H_{2'}$), 4.02 (dd, 1H, $J_{gem} = 12.8$ Hz, $J_{vic} = 6.4$ Hz, CH_2–CH=CH_2), 4.16 (dd, 1H, $J_{gem} = 12.8$ Hz, $J_{vic} = 5.4$ Hz, CH_2–CH=CH_2), 4.83 (d, 1H, $J_{1'',2''} = 1.5$ Hz, $H_{1''}$), 4.96 (d, 1H, $J_{1,2} = 1.7$ Hz, H_1), 5.21 (dd, 1H, $J_{vic} = 10.3$ Hz, $J_{gem} = 1$ Hz, CH_2–CH=CH_2), 5.28 (dd, 1H, $J_{vic} = 17.2$ Hz, $J_{gem} = 1$ Hz, CH_2–CH=CH_2), 5.91 (m, 1H, CH_2–CH=CH_2); ^{13}C NMR (500 MHz, D_2O): δ 26.5 (C3′), 26.7 (C6′), 38.9 (C4′, C5′), 52.7 (2 × OMe), 60.8 (C6), 66.7 (C5, C5″), 67.8 (C6″), 68.1 (CH_2–CH=CH_2), 68.9 (C2″), 70.2 (C3), 70.3 (C2), 70.5 (C3″), 70.8 (C2′), 71.8 (C4″), 73.2 (C4), 74.4 (C1′), 98.3 (C1), 98.9 (C1″), 118.3 (CH_2–CH=CH_2), 133.1 (CH_2–CH=CH_2); MALDI-TOF $[M+Na]^+$: 620.58.

3.2. Computational methods

All calculations were performed using the MacroModel/Batchmin[18] package (version 7.0) and the AMBER* force field with the Senderowitz-Still all-atom pyranose parameters.[19] Charges were taken from the force field (all-atom charge option) and water solvation was simulated using MacroModel's generalized Born GB/SA continuum solvent model.[20]

The conformational search was carried out using 15,000 steps of the usage directed Monte Carlo/Energy Minimization (MC/EM) procedure. The inter-glycosidic linkages and the C5–C6 bonds were used as explicit variables during the Monte Carlo search. Extended non-bonded cut off distances (a van der Waals cut off of 8.0 Å and an electrostatic cutoff of 20.0 Å) were used.

The MC/SD[21] dynamic simulations were run using the AMBER* all-atom force field and van der Waals and electrostatic cutoffs of 25 Å, together with a hydrogen bond cutoff of 15 Å. The same degrees of freedom of the MC/EM searches were used. All simulations were performed at 300 K, with a dynamic time-step of 1.5 fs and a frictional coefficient of 0.1 ps^{-1}. Runs of 5 ns each were performed, starting from conformations of the substrates, selected from the MC/EM outputs, which differed at glycosidic linkage. Structures were sampled every 3.3 ps and saved for later evaluation. The inter-atomic distances reported in Table 1 under the MC/SD header were evaluated from $<r^{-6}>$ monitored during the simulation (option MDDI of Batchmin).

Minimization of the structures saved during the dynamic simulations was performed as a multi-conformer minimization (MULT command of Batchmin), using the same energetic setup used in the MC/EM searches. The inter-atomic distances calculated from these sets

of structures are reported in Table 1 under the MC/SD/EM header. They are calculated from the Boltzmann average of the r_i^{-6} of the individual conformations found within 12 kJ/mol from the global minimum.

3.3. NMR spectroscopy

A first set of NMR data were collected on a Bruker AVANCE 500 MHz spectrometer, whereas data used for conformational analysis and those reported as Supplementary data were acquired on a Varian INOVA 800 MHz spectrometer with a 5 mm H{CN} triple probe using standard software supplied by Varian and MestreC software for data processing and spectra analysis. The sample was dissolved in 0.5 mL D_2O solutions at 295 K. Proton NMR spectrum was processed with HOD signal referenced at 4.76 ppm on proton scale. Standard heteronuclear single quantum coherence (HSQC) experiment and 2D-ROESY (mixing time 200 ms, 500 ms and 800 ms) experiments were also acquired.

Acknowledgments

We are grateful to Professor James H. Prestegard for the access to 800 MHz NMR facilities at the Complex Carbohydrate Research Center. We also thank Dr. John Glushka for his practical help and open discussion on carbohydrate behaviours. This research has been supported by the IHP European Programme under Contracts HPMT-CT-2001-00293 (Marie Curie Fellowship to I.S.-M.) and HPRN-CT-2002-00173 (Glycidic scaffolds Network).

Supplementary data

Supplementary data associated with this article can be found, in the online version, at doi:10.1016/j.carres.2007.03.019.

References

1. Sears, P.; Wong, C. H. *Angew. Chem., Int. Ed.* **1999**, *38*, 2300–2324.
2. Thomson, R.; von Izstein, M. In *Carbohydrate Based Drug Discovery*; Wong, C. H., Ed.; Wiley-VCH, 2003; Vol. 2.
3. Horstkorte, R.; Keppler, O. T.; Reutter, W. In *Carbohydrate Based Drug Discovery*; Wong, C. H., Ed.; Wiley-VCH, 2003; Vol. 2.
4. Bernardi, A.; Arosio, D.; Manzoni, L.; Micheli, F.; Pasquarello, A.; Seneci, P. *J. Org. Chem.* **2001**, *66*, 6209–6216.
5. Bernardi, A.; Brocca, P.; Checchia, A.; Sonnino, S.; Zuccotto, F. *J. Am. Chem. Soc.* **1999**, *121*, 2032–2036.
6. Bernardi, A.; Arosio, D.; Sonnino, S. *Neurochem. Res.* **2002**, *27*, 539–545.
7. Mari, S.; Posteri, H.; Marcou, G.; Potenza, D.; Micheli, F.; Cañada, F. J.; Jiménez-Barbero, J.; Bernardi, A. *Eur. J. Org. Chem.* **2004**, 5119–5225.
8. Pekari, K.; Tailler, D.; Weingart, R.; Schmidt, R. R. *J. Org. Chem.* **2001**, *66*, 7432–7442.
9. Ren, T.; Liu, D. *Tetrahedron Lett.* **1999**, *40*, 7621–7625.
10. Schmidt, R. R.; Michel, J. *Angew. Chem., Int. Ed. Engl.* **1980**, *19*, 731–732.
11. Schmidt, R. R. *Angew. Chem., Int. Ed. Engl.* **1986**, *25*, 212–235.
12. Woods, R. J.; Pathiaseril, A.; Wormald, M. R.; Edge, C. J.; Dwek, R. A. *Eur. J. Biochem.* **1998**, *258*, 372–386.
13. Wormald, M. R.; Petrescu, A. J.; Pao, Y. L.; Glithero, A.; Elliott, T.; Dwek, R. A. *Chem. Rev.* **2002**, *102*, 371–386.
14. Bernardi, A.; Colombo, A.; Sánchez-Medina, I. *Carbohydr. Res.* **2004**, *339*, 967–973.
15. Brocca, P.; Bernardi, A.; Raimondi, L.; Sonnino, S. *Glycoconj. J.* **2000**, *17*, 283–299.
16. Tian, F.; Al-Hashimi, H. M.; Craighead, J. L.; Prestegard, J. H. *J. Am. Chem. Soc.* **2001**, *123*, 485–492.
17. Mari, S.; Cañada, F. J.; Jiménez-Barbero, J.; Bernardi, A.; Marcou, G.; Motto, I.; Velter, I.; Nicotra, F.; La Ferla, B. *Eur. J. Org. Chem.* **2006**, 2925–2933.
18. Mohamadi, F.; Richards, N. G. J.; Guida, W. C.; Liskamp, R.; Lipton, M.; Caufield, C.; Chang, G.; Hendrickson, T.; Still, W. C. *J. Comp. Chem.* **1990**, *11*, 440–467.
19. Senderowitz, H.; Still, W. C. *J. Org. Chem.* **1997**, *62*, 1427–1438.
20. Still, W. C.; Tempzyk, A.; Hawley, R.; Hendrickson, T. *J. Am. Chem. Soc.* **1990**, *112*, 6127–6129.
21. Guarnieri, F.; Still, W. C. *J. Comp. Chem.* **1994**, *15*, 1302–1310.